ChemPubSoc Europe

DOI: 10.1002/cphc.201402674

Special Issue

N-Substituted Phenothiazine Derivatives: How the Stability of the Neutral and Radical Cation Forms Affects Overcharge Performance in Lithium-Ion Batteries

Kishore Anand Narayana,[a] Matthew D. Casselman,[a] Corrine F. Elliott,[a] Selin Ergun,[a] Sean R. Parkin,[a] Chad Risko,*[a, b] and Susan A. Odom*[a]

Phenothiazine and five *N*-substituted derivatives were evaluated as electrolyte additives for overcharge protection in $LiFePO_4$/synthetic graphite lithium-ion batteries. We report on the stability and reactivity of both the neutral and radical-cation forms of these six compounds. While three of the compounds show extensive overcharge protection, the remaining three last for only one to a few cycles. UV/Vis studies of redox shuttle stability in the radical cation form are consistent with the overcharge performance: redox shuttles with spectra that show little change over time exhibit extensive overcharge performance, whereas those with changing spectra have limited overcharge protection. In one case, we determined that a C–N bond cleaves upon oxidation, forming the phenothiazine radical cation and leading to premature overcharge protection failure; in another case, poor solubility appears to limit protection.

1. Introduction

The lifetimes of lithium-ion batteries (LIBs) are limited by numerous chemical and mechanical degradation mechanisms, one of which occurs when the voltage of a battery rises past its end-of-charge potential, a condition called overcharge. Compounds called redox shuttles can be incorporated into the battery electrolyte to limit cell voltage and thus prevent overcharge.[1] These compounds shuttle current through the battery electrolyte by oxidizing at the cathode/electrolyte interface, then diffusing to the anode/electrolyte interface, where reduction occurs, regenerating the neutral form. Various organic compounds and a few metallocenes and inorganic salts have been shown to protect batteries from overcharge with varying degrees of success.[2]

N-Substituted phenothiazines (PTs) were originally reported as redox shuttles for overcharge protection of LIBs in 2006 by Dahn and coworkers,[2c,3] with some derivatives exhibiting about 150 cycles of 100% overcharge when incorporated in the electrolyte of $LiFePO_4/Li_{4/3}Ti_{5/3}O_4$ coin cells. Many recent studies have focused on overcharge protection using dialkoxybenzene derivatives[2e,h,4] including some with electron-withdrawing substituents to match end-of-charge potentials for higher voltage cathodes.[2d,g] Fluorinated boronic ester[5] and lithium difluoro(oxalato)borate[2l] derivatives have also been reported as multifunctional electrolyte additives for overcharge protection. Except for derivatives reported by our group,[2m,n] PT remains an untapped aromatic core.

Although alkylated phenothiazine additives were tested with $LiFePO_4$ cathodes, the low oxidation potentials of *N*-substituted PT derivatives render them impractical for commercial application for overcharge in LIBs, and the incorporation of electron-withdrawing substituents is necessary to produce derivatives with practical (larger) oxidation potentials, as has been reported with dimethoxybenzene[2g,k] and ferrocene derivatives.[2p] Modification of the PT core is facile, and transformations can be high yielding, especially in the synthesis of derivatives with substituents at the *N* position and positions *para* to the nitrogen atom.

Using PT as a common redox-active core, our group has studied the overcharge performance of a variety of disubstituted derivatives of *N*-ethylphenothiazine (EPT).[2m,n,6] Although some EPT derivatives with substituents at the 3- and 7-positions exhibit extensive overcharge protection,[2m,n,6] we were unsure if our choice of the ethyl substituent at the *N* position was the best choice for long-lived redox shuttles. Dahn reported PT derivatives with methyl (MPT), ethyl (EPT), and isopropyl (*i*PrPT) substituents (Figure 1); little variation in performance was observed when the compounds were evaluated in side-by-side experiments in $LiFePO_4/Li_{4/3}Ti_{5/3}O_4$ coin cells.[3a] To identify the optimal substituent for the *N* position, we wanted to compare the overcharge performance of the reported PT derivatives and the unreported redox shuttle candidates PT, *N*-*tert*-butylphenothiazine (*t*BuPT), and *N*-phenylphenothiazine (PhPT) (Figure 1) in $LiFePO_4$/synthetic graphite coin cells.

In addition to evaluating the overcharge performance, we wanted to determine whether the stability of the neutral and

[a] *K. A. Narayana, Dr. M. D. Casselman, C. F. Elliott, Dr. S. Ergun, Dr. S. R. Parkin, Prof. C. Risko, Prof. S. A. Odom*
Department of Chemistry, University of Kentucky
Lexington, KY, 40506-0055 (USA)
E-mail: chad.risko@uky.edu
susan.odom@uky.edu

[b] *Prof. C. Risko*
Center for Applied Energy Research, Lexington, KY, 40511 (USA)

Supporting Information for this article is available on the WWW under http://dx.doi.org/10.1002/cphc.201402674.

An invited contribution to a Special Issue on Organic Electronics

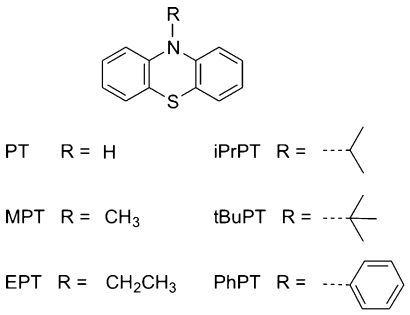

Figure 1. Phenothiazine (R = H) and its *N*-substituted derivatives (R = CH_3, CH_2CH_3, $CH(CH_3)_2$, $C(CH_3)_3$, and C_6H_5) examined in this study.

Table 1. Oxidation potentials and number of protection cycles survived in $LiFePO_4$/synthetic graphite coin cell batteries.

Redox shuttle candidate	$E_{1/2}^{+/0}$ (vs. $Cp_2Fe^{+/0}$) [V] in 0.1 M nBu_4NPF_6 in DCM	$E_{1/2}^{+/0}$ (vs. $Li^{+/0}$) [V] in 1.2 M $LiPF_6$ in EC/EMC (3:7)	Number of cycles of 100% overcharge protection[a]
PT	0.17	3.45	1, 3
MPT	0.31	3.55	3, 5
EPT	0.26	3.51	127, 139
*i*PrPT	0.33	3.59	117, 118
*t*BuPT	0.53	3.45	2, 2
PhPT	0.26	3.52	128, 161

[a] The two numbers represent the values for two batteries cycled in overcharge.

oxidized forms of the redox shuttles as dilute solutions in relatively inert organic solvents correlated with the extent of overcharge protection observed. This goal is related to our interest in predicting overcharge performance of redox shuttle candidates prior to battery fabrication.[2n,7] Understanding the stability and reactivity of redox shuttles in their neutral and oxidized states in different solvents—not necessarily those specific to the battery environment—may help to predict those candidates that will exhibit extensive overcharge protection. In addition to using UV/Vis absorption spectroscopy to monitor redox shuttle concentration in solution over time, we made use of electron paramagnetic resonance (EPR) spectroscopy and mass spectrometry to identify some of the byproducts of radical cation formation—an area that we think deserves more attention in the redox shuttle literature—and density functional theory (DFT) calculations to calculate the energies of reaction for decomposition pathways that are consistent with experimental observations.

2. Results and Discussion

2.1. Cyclic Voltammetry

We recorded cyclic voltammograms of the *N*-substituted PT derivatives in 0.1 M nBu_4NPF_6 in dichloromethane (DCM) and in 1.2 M $LiPF_6$ in ethylene carbonate/ethyl methyl carbonate (EC/EMC, 3:7 wt. ratio), a common electrolyte for LIBs. The voltammograms obtained in each electrolyte are shown in Figure 2.

Voltammograms recorded at 100 mV s^{-1} show reversible first oxidations for all derivatives. Half-wave oxidation potentials (Table 1) varied slightly with substituent. Trends in oxidation potentials generally correlate in value from one electrolyte to the other with one exception (*t*BuPT). In nBu_4NPF_6/DCM, the oxidation potential of *t*BuPT is higher than all of the derivatives, but in $LiPF_6$/EC/EMC, it is tied with PT for the lowest value.

2.2. Overcharge Performance

The overcharge performance of *N*-substituted phenothiazine derivatives was analyzed in $LiFePO_4$/synthetic graphite coin cell batteries containing 0.08 M redox shuttle in the electrolyte 1.2 M $LiPF_6$ in EC/EMC (3:7 wt. ratio). The redox shuttles (all solids) fully dissolved within a few minutes of sonication except for *t*BuPT, which took ca. 10 min to dissolve. Over-

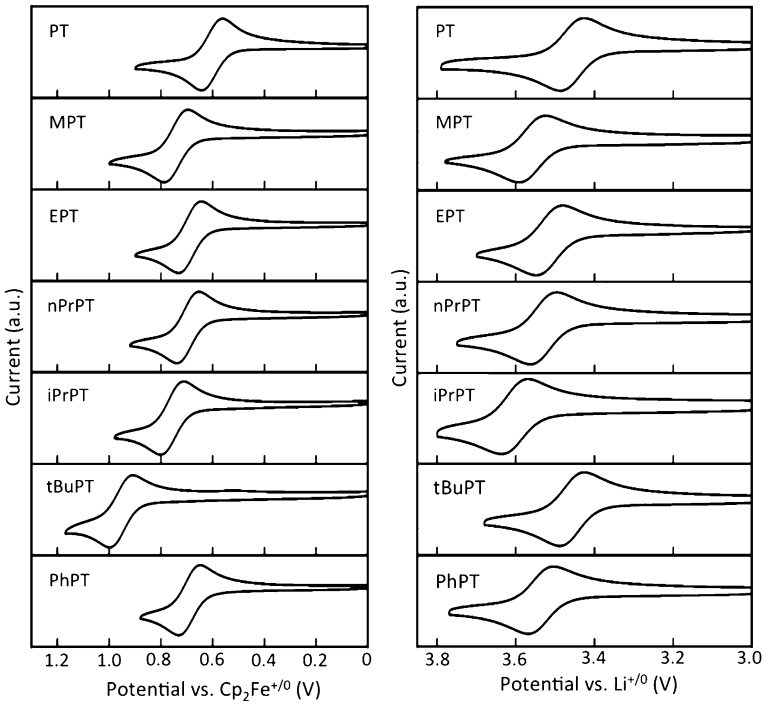

Figure 2. Cyclic voltammograms recorded at 100 mV s^{-1} showing the first oxidation observed for PT, MPT, EPT, nPrPT, *i*PrPT, *t*BuPT, and PhPT at 3×10^{-4} M in 0.1 M nBu_4NPF_6 in DCM (left) and in 1.2 M $LiPF_6$ in EC/EMC (right).

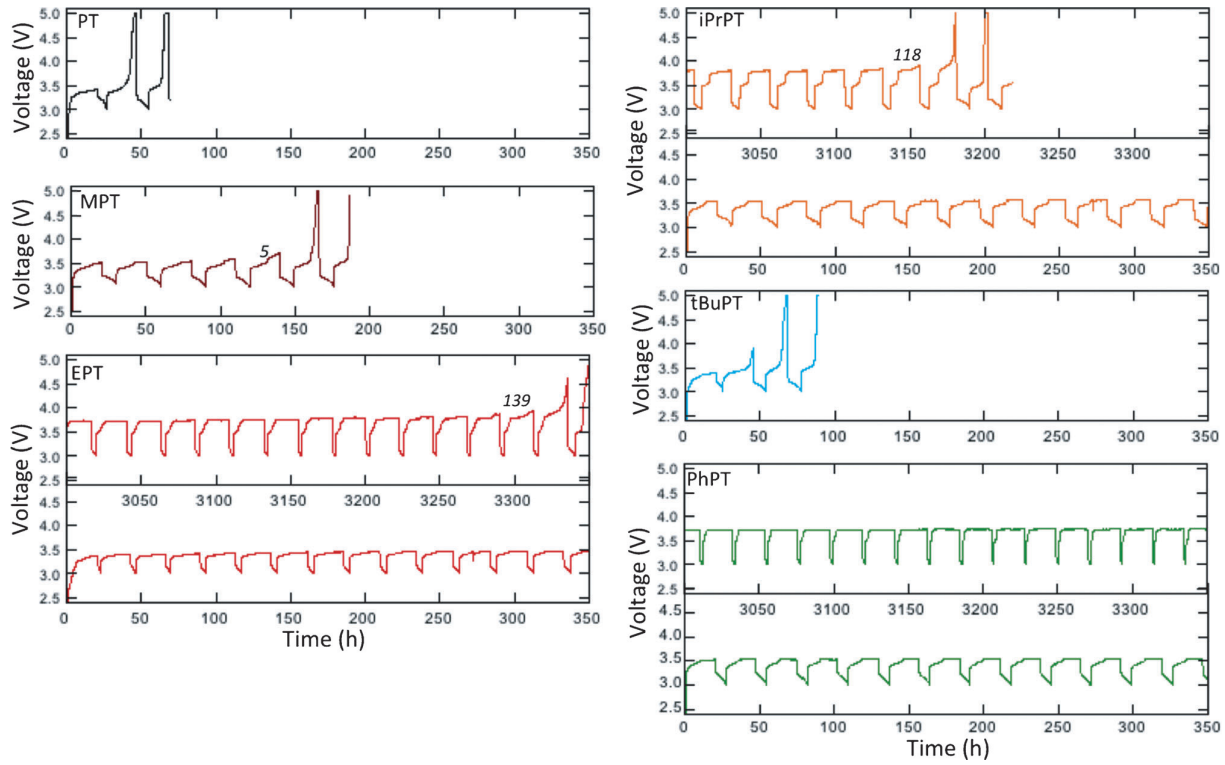

Figure 3. Voltage versus time plots of selected cycles for $LiFePO_4$/synthetic graphite coin cell batteries cycled to 100% overcharge containing PT, MPT, EPT, *i*PrPT, *t*BuPT, or PhPT at 0.08 M in 1.2 M $LiPF_6$ in EC/EMC.

charge cycling was performed by charging the coin cells to 200% of the nominal cell capacity, or 100% overcharge, at a C/10 charging rate. Specifically, this means that the coin cells were programmed to charge for 20 h (10 h in charge, 10 h in overcharge) or until 5.0 V was reached and then to discharge for 10 h or until 3.0 V was reached. Two batteries were made for each redox shuttle. Selected cycles of overcharge are shown in Figure 3, plotted as voltage vs. time. The number of cycles that each redox shuttle survived in overcharge is summarized in Table 1.

It was no surprise that PT survived for only one to three cycles of overcharge protection, as we expected this compound to be unstable as a radical cation. Aromatic cores with N–H bonds can dimerize upon oxidation to form new N–N bonds[8] or react with aromatic rings.[9] Of the *N*-substituted phenothiazines, EPT, *i*PrPT, and PhPT showed the most extensive overcharge cycling with > 100 cycles at 100% overcharge. In contrast, MPT and *t*BuPT—the derivatives with the smallest and largest steric substitution adjacent to the *N*-substituent—survived for five or fewer cycles of overcharge protection.

We were surprised that MPT exhibited so few overcharge protection cycles because Dahn's report indicated that MPT survived approximately the same number of cycles of protection (155) as EPT (150) and *i*PrPT (> 162) in $LiFePO_4/Li_{4/3}Ti_{5/3}O_4$ batteries. These results stimulated us to perform additional experiments to understand why MPT and *t*BuPT failed so rapidly in overcharge compared to the other compounds, and to understand the difference in relative oxidation potential for *t*BuPT between the two electrolytes.

2.3. Analysis of Cyclic Voltammetry and Overcharge

We examined the trends in oxidation potential for the PT derivatives. A regression line fit by least-squares to a plot of oxidation potentials in battery electrolyte versus those observed in nBu_4NPF_6/DCM shows good correlation between the oxidation potentials in each electrolyte ($R^2 = 0.98$) except for *t*BuPT, which was excluded from the fit (Figure 4a). As mentioned in Section 2.1, the oxidation potential of *t*BuPT in battery electrolyte was unexpectedly low and, notably, matched that of PT in battery electrolyte. We were prompted by this result to further explore the electrochemical properties of PT and *t*BuPT.

In addition to scanning through the first oxidation of each compound in the battery electrolyte, we continued scanning to the edge of the solvent window for PT and *t*BuPT and plotted the superimposed voltammograms in Figure 4b. When the cyclic voltammograms of PT and *t*BuPT are compared directly (first oxidation only, as well as both first and second oxidations), one can see that they are nearly identical. Additionally, the voltage vs. time plots from overcharge protection tests of PT and *t*BuPT show similarities in the behavior of these batteries (Figure 4c). Both results are consistent with *t*BuPT decomposing in the battery electrolyte to form PT, but not decomposing as a neutral compound in nBu_4PF_6/DCM.

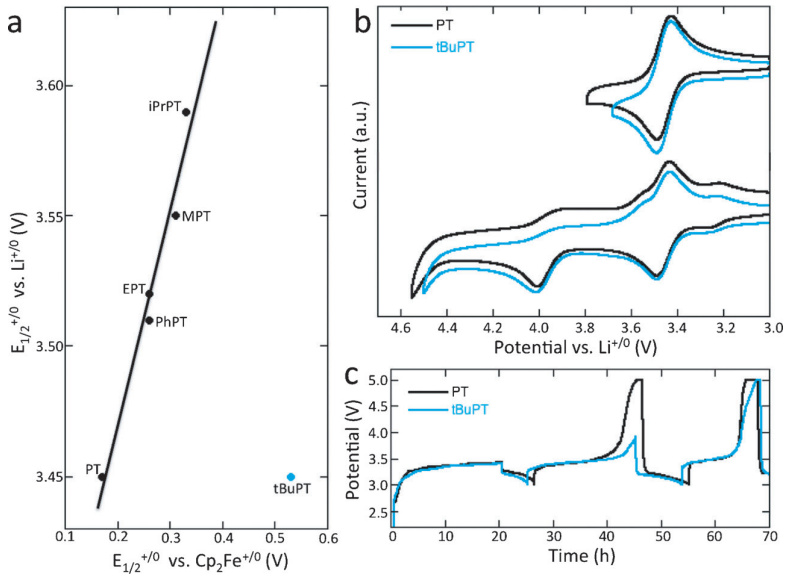

Figure 4. a) A plot of first oxidation potentials in 1.2 M $LiPF_6$ in EC/EMC (vs. $Li^{+/0}$) at 0 V versus first oxidation potentials in 0.1 M nBu_4NPF_6 in DCM (vs. $Cp_2Fe^{+/0}$) at 0 V. Cyclic voltammograms of PT and *t*BuPT in 1.2 M $LiPF_6$ in EC/EMC scanning to the first oxidations and to the second oxidations (b). Overcharge cycling of PT and *t*BuPT overlaid (c).

2.4. Redox Shuttle UV/Vis

We further explored our hypothesis by analyzing the stability of the PT derivatives by UV/Vis spectroscopy. The compounds were dissolved at 3.0×10^{-4} M in DCM, EC/EMC (3:7) or 1.2 M $LiPF_6$ in EC/EMC (3:7). The UV/Vis spectra are shown in Figure 5.

Analysis of the UV/Vis spectra showed that although the absorption spectra of most compounds were similar in shape and position in all solvents, the absorption spectrum of *t*BuPT differed significantly in $LiPF_6$/EC/EMC as compared to DCM or EC/EMC. In battery electrolyte, the absorption of the sample that contained *t*BuPT was red-shifted compared to its position in DCM or EC/EMC, instead absorbing most intensely at nearly the same wavelength as PT. As with cyclic voltammetry, the UV/Vis data suggest that *t*BuPT decomposes in battery electrolyte and forms PT; from these results, we can further infer that PT is responsible for overcharge protection in batteries fabricated with *t*BuPT, not the alkylated phenothiazine (*t*BuPT) itself.

2.5. Radical-Cation UV/Vis

Although cyclic voltammetry and UV/Vis spectroscopy provided an explanation for what happened to *t*BuPT in the battery electrolyte, the fate of MPT remained unclear. We thought the answer might lie in the stability not of its neutral form but instead of its radical-cation state. Additionally, we wanted to determine whether the stability of the radical cations in this series could be used to predict or explain redox shuttle performance across the entire series, independent of the battery environment. We suspect that if a radical cation is unstable in a solvent like DCM, then it is unlikely to be an effective redox shuttle and can be (or could have been) eliminated from battery testing. Since we have only applied this method of analysis to a few reported redox shuttles, we performed the test with the intent of fabricating batteries from all of the compounds—regardless of the result—to see whether our predictions were useful.

In this experiment, we generated radical cations in dilute solutions by treating solutions of neutral compound in DCM with 0.1 equivalents of the oxidant tris(4-bromophenyl)aminium hexachloroantimonate ($TBPA^{\bullet+}$), which was added as a more concentrated solution in DCM. An excess of neutral compound was used to ensure that the reaction with the oxidant was driven to completion. Based on our previous analysis of UV/Vis spectra of the EPT radical cation,[7] we chose to work with a radical cation concentration of 1.6×10^{-4} M; assuming complete electron transfer, this would also produce one equivalent of neutral tris(4-bromophenyl)amine, and nine equivalents of neutral PT or PT derivative would remain. These neutral compounds do not absorb beyond 400 nm, allowing the region from 400 to 1100 nm to be used for analysis of radical cation absorption spectra. The UV/Vis spectra obtained between 0 and 5 h after generation of the radical cations (symbolized by $^{\bullet+}$ following the compound abbreviation) in DCM are shown in Figure 6.

$EPT^{\bullet+}$, $iPrPT^{\bullet+}$, and $PhPT^{\bullet+}$ showed relatively little change in their spectra over the course of 5 h, indicating that their radical cations are relatively stable. These compounds survive extended overcharge cycling in $LiFePO_4$/synthetic graphite batteries. In contrast, $PT^{\bullet+}$, $MPT^{\bullet+}$, and $tBuPT^{\bullet+}$ all show changes within 5 h. The spectra for $MPT^{\bullet+}$ lost intensity over time, although their shapes did not change. We observed the formation of a fine precipitate in the cuvette from the MPT experiment.

The shapes of the absorption spectra for both $PT^{\bullet+}$ and $tBuPT^{\bullet+}$ change over time, suggesting the formation of one or more new materials that absorb in the visible region. The initial absorption spectrum of $tBuPT^{\bullet+}$ is similar to the spectra of the radical cations of *N*-alkylated PT derivatives although it is slightly red-shifted, consistent with the formation of $tBuPT^{\bullet+}$. However, within the course of 1 h, no appreciable amount of this radical cation remains. Instead, new peaks appear that show remarkable similarity to the peaks present in spectra of $PT^{\bullet+}$. This led us to the conclusion that $tBuPT^{\bullet+}$ decomposes into $PT^{\bullet+}$ when it is oxidized. However, the absorption spectrum of $PT^{\bullet+}$ also changes; this indicates that, although the species may be present upon decomposition of $tBuPT^{\bullet+}$ and

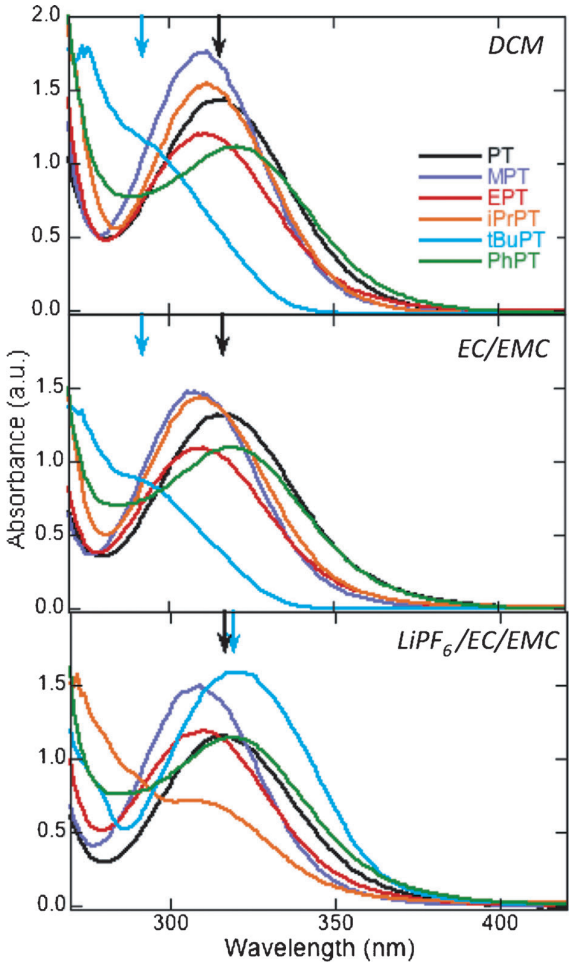

Figure 5. UV/Vis spectra of PT, MPT, EPT, *i*PrPT, *t*BuPT, and PhPT at 3.0×10^{-4} M in DCM, EC/EMC (3/7), or 1.2 M $LiPF_6$ in EC/EMC (3/7). The black arrow indicates the λ_{max} of solutions in which PT was dissolved, and the blue arrow indicates the λ_{max} of solutions in which *t*BuPT was dissolved.

after oxidation of PT, it does not remain unchanged in solution. Specifically the new peak at ca. 650 nm in both samples is not consistent with *t*BuPT$^{\bullet+}$ or PT$^{\bullet+}$. Our next experiments sought to gain more evidence that PT$^{\bullet+}$ forms after *t*BuPT$^{\bullet+}$ generation, and to determine what decomposition products formed afterward.

2.6. Radical-Cation EPR

One experiment is undeniably conclusive for the presence of radical species: electron paramagnetic resonance (EPR). In radical cations, if the lone electron has hyperfine coupling to spin-active nuclei, unique spectra can be observed. We used EPR spectroscopy to determine whether we had indeed produced radical species when oxidizing PT and *t*BuPT, and to analyze the spectra over time.

To a solution of neutral PT or neutral *t*BuPT, we added a solution of TBPA$^{\bullet+}$, thereby generating a solution of about 1.6×10^{-4} M in DCM (assuming complete electron transfer). Spectra collected as soon as possible after radical cation generation and another set collected at 10 min after generation are shown for both samples in Figure 7.

In these plots, one can see that although the EPR spectra—plotted as a derivative of signal intensity—are considerably different upon initial generation, the spectra at 10 min resemble each other. Although the intensities of the peaks do not match exactly, the number and position of peaks are generally similar between the samples, again consistent with the hypothesis that *t*BuPT$^{\bullet+}$ decomposes to form PT$^{\bullet+}$.

2.7. Bulk Electrolysis and Mass Spectrometry

Although EPR spectroscopy is useful for comparing samples and analyzing solutions containing primarily one material, we needed more specific experiments for structural identification of the product(s) that led to the peak at about 650 nm in the UV/Vis spectra. To analyze the products that form upon decomposition of *t*BuPT$^{\bullet+}$, we used mass spectrometry; we thought this technique would be most appropriate for a potential combination of products that would not necessarily be formed in high yield or be easy to separate. Although we could use the remnants from UV/Vis or EPR experiments for mass spectrometry, these samples were complicated by having an excess of neutral PT derivative present and by containing the neutral form of the chemical oxidant. We therefore elected to use bulk electrolysis to produce samples for mass spectrometry. In this way, we could also analyze larger amounts of sample without requiring large amounts of oxidant.

Bulk electrolysis experiments of *t*BuPT were performed in $n\mathrm{Bu_4NPF_6}$/DCM solutions with a reticulated vitreous carbon (RVC) working electrode, Pt coiled-wire counter electrode and Ag/AgCl reference electrode. A potential was applied until 1.00 e^-/mol was consumed, after which *N,N*-dimethylformamide (DMF) was added to the solution to serve as a base. After isolation of the organic products and purification by column chromatography, we identified one fraction as PT by ^{1}H NMR; another fraction that contained a mixture of products, which we analyzed by electrospray ionization mass spectrometry (ESI-MS). We chose this technique because it tends to not fragment ions, rendering it useful for the analysis of samples in which multiple components may be present.

The mass spectrum collected from this sample is shown in Figure 8 along with a proposed decomposition mechanism of *t*BuPT$^{\bullet+}$. Significant observed peaks have mass-to-charge (*m/z*) ratios of 395, 451, and 592, which are consistent with the formation of a dimer of PT, a PT dimer containing a *tert*-butyl group, and a PT trimer, respectively. Structures of possible decomposition products are shown below; without further characterization, we cannot know if these structures are correct or if the products are isomers of those drawn in Figure 8, but the structures are consistent with those isolated or predicted by others studying reactions of PT$^{\bullet+}$.[9]

We hypothesize that the reason for the limited performance of MPT$^{\bullet+}$ is different from that of *t*BuPT$^{\bullet+}$ as the MPT$^{\bullet+}$ UV/Vis absorption spectrum does not change shape over time, in contrast to *t*BuPT$^{\bullet+}$ where a new species appears. For MPT$^{\bullet+}$,

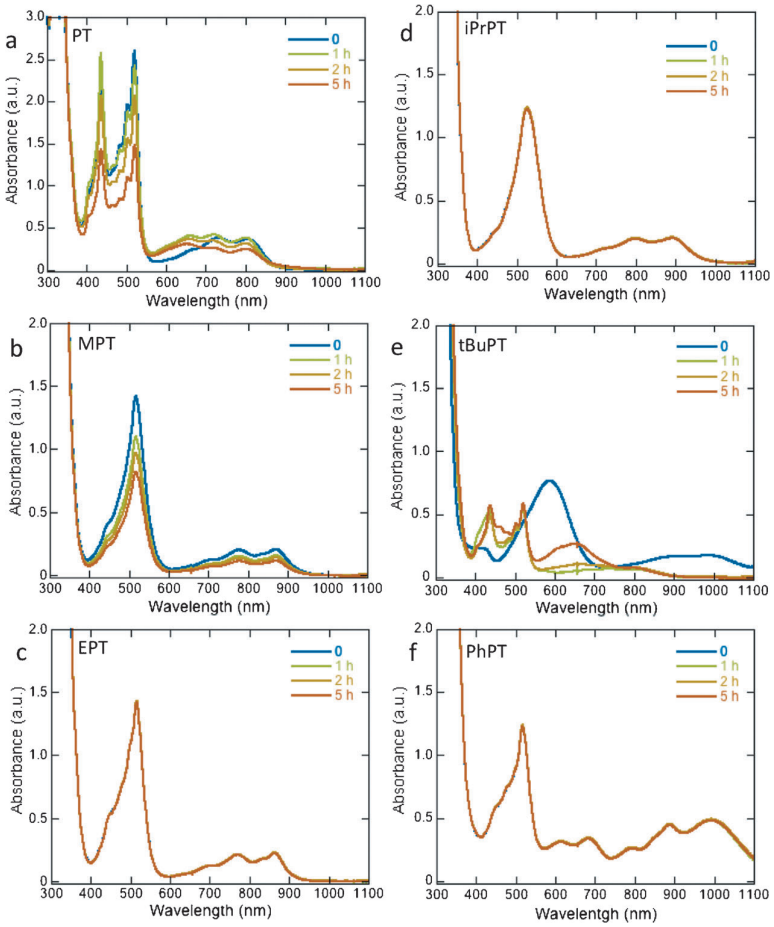

Figure 6. UV/Vis of the products of the reaction of the chemical oxidant $TBPA^{\bullet+}$ with solutions of PT (a), MPT (b), EPT (c), *i*PrPT (d), *t*BuPT (e), and PhPT (f) at 0, 1, 2, and 5 h, radical cations generated in DCM at 1.6×10^{-4} M.

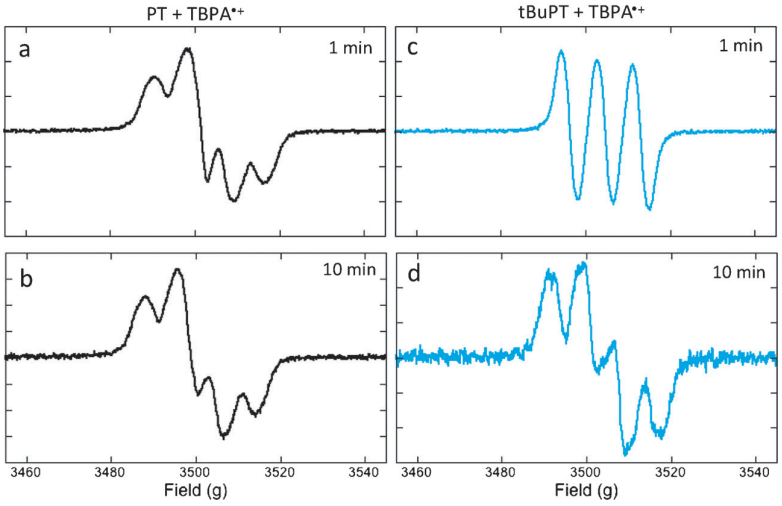

Figure 7. EPR spectra of dichloromethane solutions of *t*BuPT and PT generated at 1.6×10^{-4} M after treatment with the chemical oxidant $TBPA^{\bullet+}$ at about 1 min after mixing (*t*BuPT, a; PT, c) and about 10 min after mixing (*t*BuPT, b; PT, d).

it was unclear if the loss in intensity is due to limited stability or solubility. From UV/Vis data, we know that it is not decomposing to the $PT^{\bullet+}$ (at least, not at an appreciable rate) because we do not see the peaks characteristic of this species, which were observed in the decomposition of $t\text{BuPT}^{\bullet+}$. We thought that bulk electrolysis at higher concentrations in battery electrolyte would lead us to a clearer picture of what was happening with MPT. We dissolved MPT at 0.08 M in 1.2 M $LiPF_6$ in EC/EMC (the same concentration as we employ in our batteries) and carried out bulk electrolysis at 3.8 V (vs. $Li^{+/0}$) until 1 e^-/mol was passed through the solution. A dark solid formed and was isolated as a finely divided green, leaving behind a deep red solution. The organic solution was analyzed by TLC and GC-MS; by either technique, only MPT was observed. A similar experiment was conducted on EPT. No solid formed during bulk electrolysis, and TLC analysis showed no new products at the conclusion of the reaction. Thus neither $MPT^{\bullet+}$ nor $EPT^{\bullet+}$ form new soluble products during bulk electrolysis in battery electrolyte, but $MPT^{\bullet+}$ precipitates where $EPT^{\bullet+}$ does not at the same concentration; these results suggest that $MPT^{\bullet+}$ is less soluble than $EPT^{\bullet+}$, which could explain why MPT does not survive as long in overcharge.

2.8. Molecular Geometry and Reactivity

To better understand the stability and reactivity of the PT derivatives, specifically *t*BuPT, we undertook a study of the neutral and radical-cation forms using density functional theory (DFT) at the B3LYP/6-311G(d,p) level. All PT derivatives are bent symmetrically through the N and S atoms, a trait referred to as the

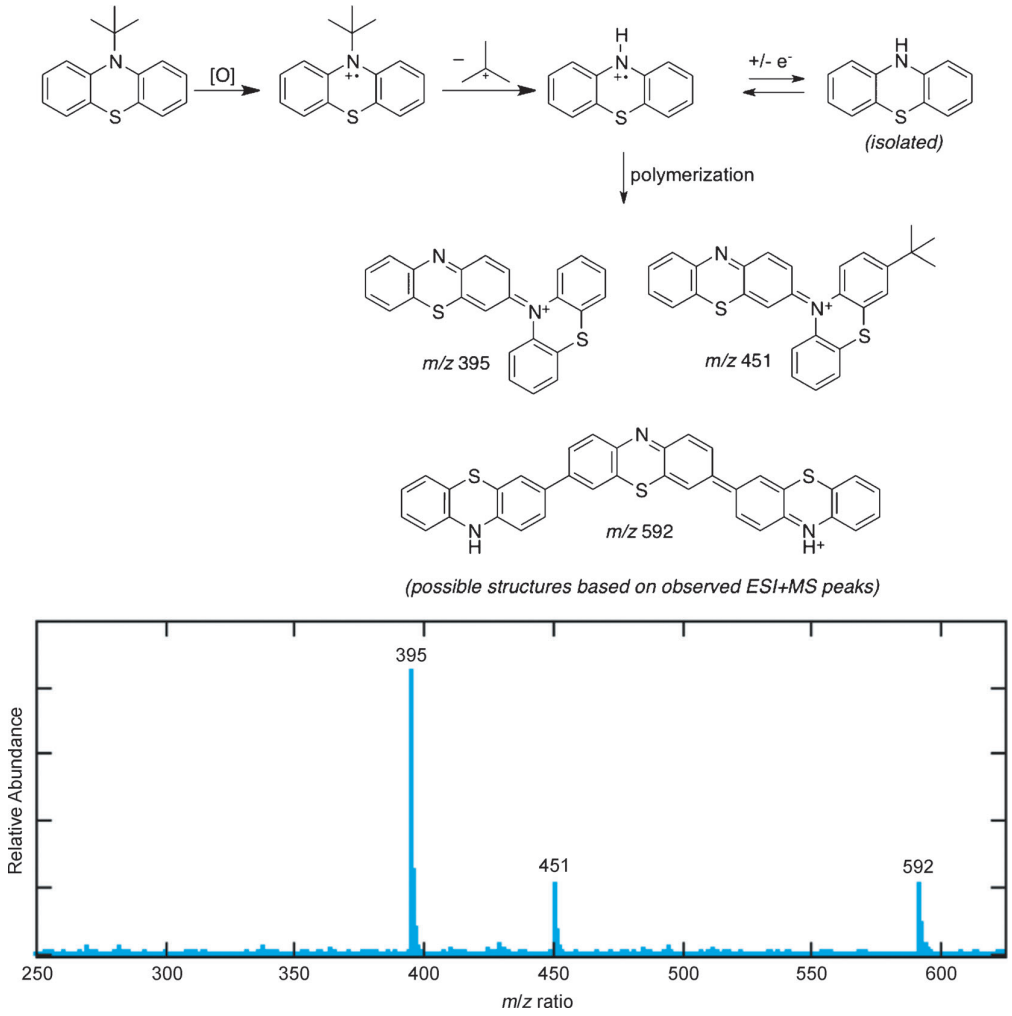

Figure 8. Proposed decomposition of *t*BuPT$^{\bullet+}$ and ESI mass spectrum of products isolated following bulk electrolysis.

"butterfly angle" (defined as the angle formed by the intersection of the aryl-ring planes). Notably, the DFT-determined molecular (neutral and radical cation) geometries of PT and its alkylated derivatives closely match those of reported crystal structures[10] and of crystals grown in our laboratory. Representative crystal-structure and DFT-derived molecular geometries for the neutral and radical cation forms of EPT and *t*BuPT are shown in Figure 9.

The neutral PT derivatives are substantially bent, with butterfly angles ranging from 135° to 150°. The radical cations, on the other hand, are more planar, with butterfly angles that range from 148° to 180° (fully planar). (We note that crystal structures are not available for *i*PrPT$^{\bullet+}$, *t*BuPT$^{\bullet+}$, or PhPT$^{\bullet+}$; see Table S2 for a summary of calculated and experimental butterfly angles.) Although the geometries of most PT derivatives show a fairly large difference between the neutral and radical cation butterfly angles (i.e. as much as 30° for PT and PhPT), the butterfly angle in *t*BuPT, the derivative with the bulkiest alkyl substituent considered, changes by only 14° (from 134° neutral to 148° radical cation) upon oxidation. The large *tert*-butyl group hinders the PT ring system from moving to the planar configuration favored by other PT radical cations, which constrained-geometry calculations reveal to be an energetically unfavorable state that results in an uncharacteristically long C–N bond between PT and the *tert*-butyl group (see Figure S1 and the SI for more details).

Experimental work shows that *t*BuPT$^{\bullet+}$ is the least stable radical cation in the series, perhaps because it has the most constrained radical-cation geometry. We calculated the energies of reaction for several potential decomposition pathways and, based on the reaction energy being the most negative, we propose that *t*BuPT$^{\bullet+}$ readily decomposes via a low-energy fragmentation pathway into PT$^{\bullet+}$ and isobutylene (Scheme 1, first reaction). A comparison of the (gas-phase) alkene decomposition reactions across the alkylated PT series reveals that the only energetically favorable reaction is the formation of the isobutylene byproduct with a zero-point energy [ZPE] corrected reaction energy of $\Delta E = -6.35$ kcal mol^{-1} (see Table S3 in the SI for a table of energies of reaction). Use of a solvent-continuum model (formic acid, $\varepsilon = 51.1$) to represent the polar-

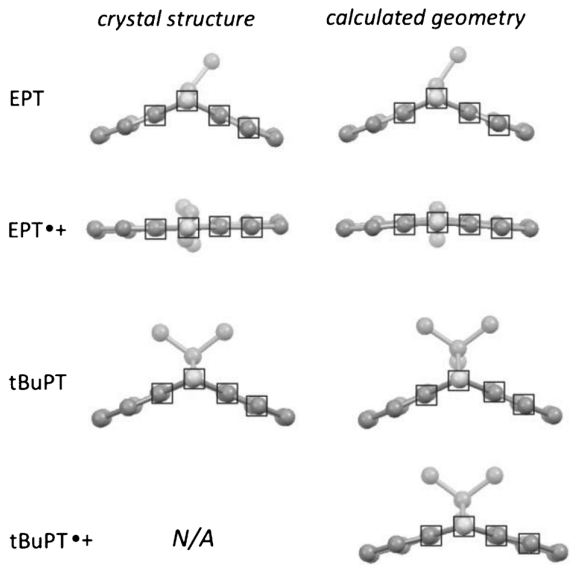

Figure 9. Crystal structures (left) and optimized molecular geometries at the B3LYP/6-311G(d,p) level of theory (right) for the neutral and radical-cation forms of EPT and *t*BuPT. A crystal structure for the *t*BuPT radical cation has not been reported.

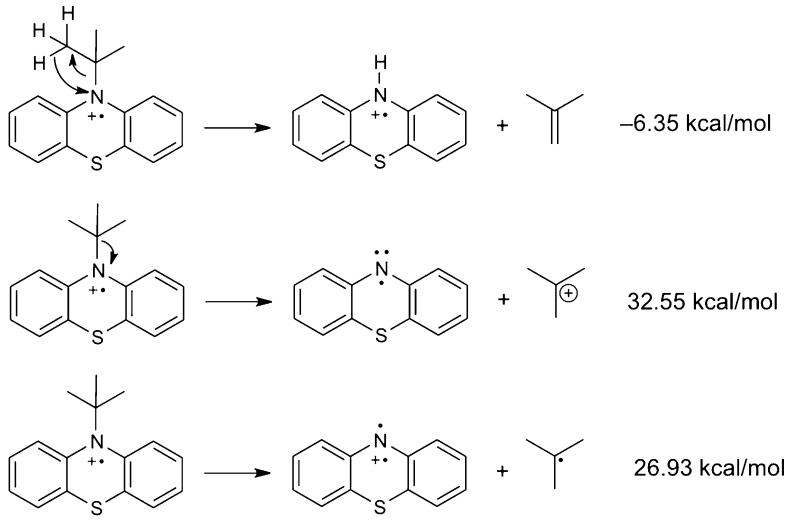

Scheme 1. Proposed decomposition pathways of *t*BuPT$^{\bullet+}$. Zero-point corrected energies of reaction (gas-phase) computed at the B3LPY/6-311G(d,p) level of theory are also provided.

izable environment of the battery electrolyte resulted in a downward shift of the energies for all reactions considered, as expected, with the PT$^{\bullet+}$ and isobutylene decomposition products being the most favorable. Notably, the decomposition reaction of *i*PrPT to PT$^{\bullet+}$ and propene becomes modestly favorable ($\Delta E = -0.68$ kcal mol^{-1}) when the solvent-continuum is taken into account; this result correlates with the *i*PrPT radical cation having a comparatively bent structure, with a butterfly angle of 161°. The energies for alternate decomposition pathways that would produce either the carbocation or the radical of the *tert*-butyl substituent (Scheme 1, second and third reactions) were also considered, but these cleavage reactions (in both the gas-phase and solvent continuum) are significantly higher-energy decomposition pathways.

The UV/Vis and EPR studies of the radial-cations reveal that *t*BuPT, in stark contrast to the other alkylated PTs, decomposes to a product that has many features reminiscent of PT$^{\bullet+}$. Consistent with these results, the theoretical analysis of potential decomposition pathways suggests that the *tert*-butyl group may be readily eliminated as isobutylene after oxidation. The combined experimental and theoretical results point to important considerations concerning the chemistry of redox shuttles, which need to be contemplated in future molecular design protocols.

3. Conclusions

Subtle changes in structure can have dramatic effects on the performance of a redox shuttle during overcharge protection of LIBs. Although it is widely agreed that the stability of the radical cation form of a redox shuttle is the key factor governing the stability of the compound in battery electrolyte, we found that in one case, a redox shuttle candidate decomposed in battery electrolyte before ever experiencing overcharge, yet protected for as many cycles at the same potential as the product we identified that it forms; hence, the stability of the neutral redox shuttle is also important to consider. In three cases, radical-cation instability was consistent with limited overcharge cycling, and in the remaining three cases, compounds with highly stable radical cations showed extended overcharge cycling.

Although not explored in this publication, additional important factors for redox shuttles include diffusion coefficients and solubility, both of which are often sensitive to the electrolytes employed and the concentration of electrolyte salts. None of these factors can be ignored; reaching an ideal solution may not be a matter of focusing on one problem, but rather balancing stability and physical properties. Although most of the decomposition products of aromatic redox shuttles are redox active, it is difficult to know if the products are responsible for overcharge protection unless they are synthesized and tested separately.

From the substituents investigated at the *N* position of PT, we have learned that while it is important to have a non-hydrogen substituent, it is important to consider the chemical nature of the substituent, that is, the substituent shoud *not* be

a *tert*-butyl group as steric bulk prevents the formation of a stable, alkylated PT radical cation (although this result does *not* mean *tert*-butyl groups should not be used in other systems). Notably, the as yet unexplored phenyl substituent leads to the most robust redox shuttle under consideration. As a result of these experiments, we plan to incorporate the phenyl substituent onto other PT derivatives that have shown extended overcharge performance with ethyl substituents at the *N* position in order to determine whether derivatives of these redox shuttles will likewise display extended overcharge protection.

We hope that our future work will allow us to hone in on the most important factors contributing to long-term overcharge performance. We realize that some of these results will impact not only additives for overcharge protection but may also be helpful for other energy-storage applications such as non-aqueous redox flow batteries, for which similar compounds are of interest as electro-active materials for the positive side of the battery.[11]

Experimental Section

General

PT and MPT were purchased from Sigma Aldrich and were crystallized from pentane. EPT was synthesized as previously reported.[7] Bis(2-bromophenyl)sulfane[12] and PhPT[13] were synthesized following procedures similar to those used for the previously-reported compounds. *i*PrPT and *t*BuPT were synthesized from bis(2-bromophenyl)sulfane using a modified Buchwald-Hartwig coupling reaction.[14] See the SI for synthetic procedures.

Sodium hydride was purchased from Alfa Aesar. Potassium carbonate, copper powder, tetra(*n*-butyl)ammonium hexafluorophosphate (nBu$_4$NPF$_6$), and tris(4-bromophenyl)aminium hexachloroantimonate were purchased from Sigma Aldrich. Iodobenzene, isopropyl amine, *tert*-butyl amine, sodium sulfide nonahydrate, 1-bromo-2-iodobenzene, bis(dibenzylideneacetone)-palladium (Pd(dba)$_2$), ±-2,2′-bis(diphenylphosphino)-1,1′-binaphthyl (±-BINAP), and copper(I) iodide were purchased from Acros Organics. Silica gel (65×250 mesh) was purchased from Sorbent Technologies. Anhydrous solvents and solvents for product purification were purchased from Fisher Scientific. Ethylene carbonate, ethyl methyl carbonate, and lithium hexafluorophosphate were purchased from BASF Corporation (NJ, USA). ^{1}H and ^{13}C NMR spectra were obtained on Varian spectrometers in [D$_6$]DMSO or CDCl$_3$ from Cambridge Isotope Laboratories. Mass spectra were obtained on an Agilent 5973 Network mass selective detector attached to Agilent 6890N Network GC system or through ESI for which samples were dissolved in acetonitrile/water (2:1) before analysis. Electrospray ionization (ESI) mass spectra were obtained on a Thermo Finnigan LTQ (ion trap mass spectrometer), with sample introduction by direct infusion (syringe pump) at 3 μL min^{-1}. Full scan mass spectra were recorded in positive ion mode. Instrument parameters included spray voltage: 3.5 kV, capillary temperature: 185 °C, capillary voltage: 50 V, and tube lens voltage: 80 V.

Cyclic Voltammetry

Cyclic voltammetry experiments were performed using a three-electrode setup on a CH Instruments 600D potentiostat at concentrations of 3.0×10^{-4} M in analyte and at 100 mV s^{-1}. Ferrocene was added as an internal standard in all cases. In both electrolytes, glassy carbon was the working electrode, and platinum was the counter electrode. In 0.1 M nBu$_4$NPF$_6$ in anhydrous DCM, freshly anodized Ag/AgCl was used as the reference electrode, and voltammograms were referenced to ferrocenium/ferrocene ($Cp_2Fe^{+/0}$) at 0 V. For voltammograms obtained in 1.2 M LiPF$_6$ in EC/EMC (3:7 wt. ratio), experiments were performed in an argon-filled glove box, the reference was Li metal, and voltammograms were referenced to $Li^{+/0}$ at 0 V.

Battery Fabrication

Lithium iron phosphate (LiFePO$_4$) cathodes were purchased from Piotrek (Japan). The synthetic graphite anode, also termed as 'Gen 2 anode', was supplied by Argonne National Laboratory, along with 2032 coin cell battery components including battery case (upper and lower caps), spacers and gaskets. Gen-2 anode was composed of 92 wt.% MAG-10 graphite (Hitachi) as the active material and 8 wt.% polyvinylidene fluoride as the binder. The trilayer polymer separator Celgard 2325 was donated by Celgard (Charlotte, USA). 2032 LiFePO$_4$/synthetic graphite coin cell batteries were assembled in an argon-filled glove box and contained an electrolyte consisting of 0.08 M redox shuttle in 1.2 M LiPF$_6$ in EC/EMC (3:7 wt. ratio).

Overcharge Cycling

Battery cycling experiments were performed on a Maccor 4200 Battery Cycler. The battery cycling procedure involved charging the coin cells with constant current C/10 for 20 h (100% overcharge) or until a specific upper voltage (5.0 V) was reached. If the voltage of the coin cell did not reach 5.0 V after 20 h, the charging step was followed by a 30 s rest and discharging to 3.0 V with the same current rate. If a coin cell reached an upper voltage of 5.0 V, cycling was stopped.

UV/Vis Spectra

UV/Vis spectra were obtained using optical glass cuvettes (Starna) with 1 cm path length on an Agilent 8453 diode array spectrometer. UV/Vis spectra for the neutral compounds were obtained in DCM, in 0.1 M EC/EMC (3:7 wt. ratio), and in 1.2 M LiPF$_6$ in EC/EMC (3:7 wt. ratio) at 3.0×10^{-4} M.

UV/Vis spectra of the radical cations were obtained in anhydrous DCM. In each case, 1.0 mL of a solution of TBPA$^{\bullet+}$ in DCM (5.0×10^{-4} M) was added to 2.0 mL of a solution of phenothiazine in DCM (2.5×10^{-3} M) to make a final concentration in each cuvette of 1.6×10^{-4} M oxidant and 1.6×10^{-3} M analyte. The cuvette was immediately capped with a Teflon stopper and rotated to distribute the oxidant throughout the sample. Assuming complete electron transfer, the combination of oxidant and analyze would produce 1.6×10^{-4} M in radical cation, 1.6×10^{-4} M in neutral oxidant, and 1.44×10^{-3} M remaining neutral phenothiazine. Spectra were recorded at various times from 0–5 h.

Electron Paramagnetic Resonance (EPR) spectroscopy

EPR spectra were obtained using 4 mm quartz EPR tubes (Wilmad) on an X-band Bruker EPR spectrometer. For generating the radical cations of PT and *t*BuPT, the same amounts and concentrations of neutral redox shuttle and oxidant were combined and transferred

to the EPR tube as were used in the UV/Vis studies of radical cations. Initial spectra were obtained in about 1 min of oxidant addition, which was followed by an acquisition at about 10 min following oxidant addition.

Bulk Electrolysis

*t*BuPT (25.5 mg, 0.100 mmol) was dissolved in a 50 mM solution of nBu$_4$NPF$_6$ in DCM (50 mL). Bulk electrolysis of the sample was conducted using an RVC working electrode, a Pt coiled-wire counter electrode and a freshly anodized Ag/AgCl reference electrode. A potential of 0.95 V (relative to Ag/AgCl) was applied until 1.00 F mol^{-1} was consumed. During this time, the solution turned dark red/brown in color. Following electrolysis, DMF (5 mL) was added to the reaction mixture. The solution turned deep green in color. The reaction was stirred for 30 min at room temperature. The organic mixture was then washed with saturated aqueous sodium thiosulfate and brine, and then concentrated to a reduced volume (ca. 5 mL). Diethyl ether (50 mL) was added to precipitate salts, and the sample was dried over $MgSO_4$, filtered, and concentrated to dryness. The residue was purified by column chromatography using 0–10% MeOH/DCM eluent to afford unsubstituted phenothiazine (14 mg). A fraction containing a mixture of intensely-colored compounds and TBA salts was also obtained and analyzed by ESI-MS.

MPT (203 mg) was dissolved at 0.08 M in 1.2 M $LiPF_6$ in EC:EMC (3:7, 12 mL). A fritted glass tube was placed in a vial and 1 mL of solution was added to the fritted tube, and the vial was filled with solution to the same level as that of the tube. A platinum coil was used as a working electrode in the fritted tube; the counter electrode was a platinum wire and the reference electrode was lithium metal. Bulk electrolysis at 3.8 V (vs. $Li^{+/0}$) was carried out until 7.72 C (1 equiv e$^-$/mol) of electricity was passed through solution. A dark solid formed in the fritted tube. The radical cation solution and solid were pipetted out. The solid was filtered to afford a finely divided green solid. The solution was deep red in color. An aliquot of the solution was diluted with dichloromethane and washed with aqueous $NaHSO_3$. The organic layer was analyzed by TLC and GC-MS. No new products were formed. The same experiment was repeated with EPT. No solid formed during bulk electrolysis and TLC analysis showed no new products at the conclusion of the reaction.

X-ray Crystallography

Crystal structures were obtained by single-crystal X-ray diffraction for EPT, *i*PrPT, *t*BuPT, and PhPT. Crystallographic data for some neutral compounds were obtained from published data including those of PT,[15] MPT,[16] EPT,[17] *i*PrPT,[18] and PhPT[19] as well as those of the radical cations of PT,[10a,b] MPT,[10c] and EPT.[10d]

DFT Calculations

All density functional theory (DFT) calculations were performed using the Gaussian09 (Revision A.02b) software suite.[20] Geometry optimizations of the neutral and radical-cation states were carried out with the B3LYP functional[21] and 6–311G(d,p) basis set. Frequency analyses of all (fully relaxed) optimized geometries were undertaken to ensure that the geometries were energetic minima. The energy of each decomposition pathway was obtained from energies for each product/reactant computed at the same level of theory.

Optimizations of restricted geometries were performed with the B3LYP functional alternately using 6–31G(d,p), 6–311G(d,p) and cc-pVTZ basis sets. For each of these calculations, the dihedral angles on the phenothiazine core of *t*BuPT (radical cation) were frozen at $\pm 180^\circ$ (using opt = modredundant). Bond lengths and angles within the phenothiazine core were allowed to optimize, as was the entirety of the alkyl group.

Acknowledgements

We thank the University of Kentucky's Office for the Vice President for Research and the College of Arts and Sciences, the American Chemical Petroleum Research Fund, and the National Science Foundation, Division of Chemistry for Award Number CHE-1300653 for funding for this research. We thank the University of Kentucky's High Performance Computing Facility for supercomputer access. We also thank Andrew Jansen and Bryant Polzin at the Cell Manufacturing and Modeling Center at Argonne National Laboratory for battery cycler supplies, battery electrodes, and helpful advice.

Keywords: overcharge protection · phenothiazine · radical cations · redox shuttles · substituent effects

[1] a) Q. Wang, S. M. Zakeeruddin, I. Exnar, M. Graetzel, *Electrochem. Commun.* **2008**, *10*, 651–654; b) Z. Chen, Y. Qin, K. Amine, *Electrochim. Acta* **2009**, *54*, 5605–5613.

[2] a) C. Buhrmester, L. M. Moshurchak, R. L. Wang, J. R. Dahn, *J. Electrochem. Soc.* **2006**, *153*, A1800–A1804; b) J. K. Feng, X. P. Ai, Y. L. Cao, H. X. Yang, *Electrochem. Commun.* **2007**, *9*, 25–30; c) L. M. Moshurchak, C. Buhrmester, R. L. Wang, J. R. Dahn, *Electrochim. Acta* **2007**, *52*, 3779–3784; d) L. Zhang, Z. Zhang, H. Wu, K. Amine, *Energy Environ. Sci.* **2011**, *4*, 2858–2862; e) W. Weng, Y. Tao, Z. Zhang, P. C. Redfern, L. A. Curtiss, K. Amine, *J. Electrochem. Soc.* **2013**, *160*, A1711–A1715; f) Y. Zhang, L. Wang, A. Zhang, C. Zhang, P. Zhang, *Ionics* **2011**, *17*, 421–427; g) L. M. Moshurchak, W. M. Lamanna, M. Bulinski, R. L. Wang, R. R. Garsuch, J. Jiang, D. Magnuson, M. Triemert, J. R. Dahn, *J. Electrochem. Soc.* **2009**, *156*, A309–A312; h) L. Zhang, Z. Zhang, P. C. Redfern, L. A. Curtiss, K. Amine, *Energy Environ. Sci.* **2012**, *5*, 8204–8207; i) M. N. Golovin, D. P. Wilkinson, J. T. Dudley, D. Holonko, S. Woo, *J. Electrochem. Soc.* **1992**, *139*, 5–10; j) Z. Chen, J. Liu, A. N. Jansen, G. GirishKumar, B. Casteel, K. Amine, *Electrochem. Solid-State Lett.* **2010**, *13*, A39–A42; k) Z. Chen, A. N. Jansen, K. Amine, *Energy Environ. Sci.* **2011**, *4*, 4567–4571; l) Z. Chen, Y. Ren, A. N. Jansen, C.-k. Lin, W. Weng, K. Amine, *Nat. Commun.* **2013**, *4*, 1513; m) S. Ergun, C. F. Elliott, A. P. Kaur, S. R. Parkin, S. A. Odom, *Chem. Commun.* **2014**, *50*, 5339–5341; n) S. Ergun, C. F. Elliott, A. P. Kaur, S. R. Parkin, S. A. Odom, *J. Phys. Chem. C* **2014**, *118*, 14824–14832; o) K. M. Abraham, D. M. Pasquariello, E. B. Willstaedt, *J. Electrochem. Soc.* **1990**, *137*, 1856–1857; p) K. M. Abraham, *J. Electrochem. Soc.* **2012**, *159*, A1057–A1064.

[3] a) C. Buhrmester, L. Moshurchak, R. L. Wang, J. R. Dahn, *J. Electrochem. Soc.* **2006**, *153*, A288–A294; b) J. R. Dahn, C. Buhrmester, R. L. Wang, W. M. Lamanna, *U. S. Patent US7615312 B2* **2009**.

[4] J. C. Forgie, D. Rochefort, *RSC Adv.* **2013**, *3*, 12035–12038.

[5] Z. Chen, K. Amine, *Electrochem. Commun.* **2007**, *9*, 703–707.

[6] A. P. Kaur, S. Ergun, C. F. Elliott, S. A. Odom, *J. Mater. Chem. A,* manuscript accepted.

[7] S. A. Odom, S. Ergun, P. P. Poudel, S. R. Parkin, *Energy Environ. Sci.* **2014**, *7*, 760–767.

[8] S. R. Waldvogel, B. Janza, *Angew. Chem. Int. Ed.* **2014**, *53*, 7122–7123; *Angew. Chem.* **2014**, *126*, 7248–7249.

[9] a) P. Hanson, R. O. C. Norman, *J. Chem. Soc. Perkin Trans. 2* **1973**, 264–271; b) O. B. Tomilin, E. P. Konovalova, V. N. Yuzhalkin, L. V. Ryabkina, E. P. Sanaeva, *Chem. Heterocyc. Compd.* **1996**, *32*, 365–370; c) H. J. Shine, J. J. Silber, R. J. Bussey, T. Okuyama, *J. Org. Chem.* **1972**, *37*, 2691–2697;

d) L. G. Shagun, I. A. Dorofeev, I. A. Tokareva, V. I. Smirnov, V. A. Shagun, M. G. Voronkov, *Russ. J. Org. Chem.* **2012**, *48*, 1263 – 1264.

[10] a) T. Uchida, M. Ito, K. Kozawa, *Bull. Chem. Soc. Jpn.* **1983**, *56*, 577 – 582; b) S. V. Rosokha, J. K. Kochi, *J. Am. Chem. Soc.* **2007**, *129*, 3683 – 3697; c) Q. Wang, L. Youcheng, D. Yangbing, L. Zhongli, *Chin. J. Struct. Chem.* **1988**, *7*, 153; d) L. Youcheng, D. Yanbing, L. Zhongli, W. Qiguang, *Chin. J. Struct. Chem.* **1989**, *8*, 140.

[11] a) Z. Li, S. Li, S. Liu, K. Huang, D. Fang, F. Wang, S. Peng, *Electrochem. Solid-State Lett.* **2011**, *14*, A171 – A173; b) F. R. Brushett, J. T. Vaughey, A. N. Jansen, *Adv. Energy Mater.* **2012**, *2*, 1390 – 1396; c) L. Su, M. Ferrandon, J. A. Kowalski, J. T. Vaughey, F. R. Brushett, *J. Electrochem. Soc.* **2014**, *161*, A1905 – A1914.

[12] Y. Li, C. Nie, H. Wang, X. Li, F. Verpoort, C. Duan, *Euro. J. Org. Chem.* **2011**, 7331 – 7338.

[13] Y. Ahn, D. E. Jang, Y.-B. Cha, M. Kim, K.-H. Ahn, Y. C. Kim, *Bull. Korean Chem. Soc.* **2013**, *34*, 107 – 111.

[14] S. Hong, S. Hwimin, *Vol. US 2012/0059182A1*, University of Florida Research Foundation, United States, **2012**.

[15] J. McDowell, *Acta Crystallogr. Sect. B* **1976**, *32*, 5 – 10.

[16] S. S. C. Chu, D. Van der Helm, *Acta Crystallogr. Sect. B* **1974**, *30*, 2489 – 2490.

[17] S. S. C. Chu, D. Van der Helm, *Acta Crystallogr. Sect. B* **1975**, *31*, 1179 – 1183.

[18] S. S. C. Chu, D. Van der Helm, *Acta Crystallogr. Sect. B* **1976**, *32*, 1012 – 1016.

[19] C. L. Klein, J. M. Conrad, III, S. A. Morris, *Acta Crystallogr. Sect. C* **1985**, *41*, 1202 – 1204.

[20] Gaussian 09 (Revision A.02b), M. J. Frisch, G. W. Trucks, H. B. Schlegel, G. E. Scuseria, M. A. Robb, J. R. Cheeseman, G. Scalmani, V. Barone, B. Mennucci, G. A. Petersson, H. Nakatsuji, M. Caricato, X. Li, H. P. Hratchian, A. F. Izmaylov, J. Bloino, G. Zheng, J. L. Sonnenberg, M. Hada, M. Ehara, K. Toyota, R. Fukuda, J. Hasegawa, M. Ishida, T. Nakajima, Y. Honda, O. Kitao, H. Nakai, T. Vreven, J. A. Montgomery, Jr., J. E. Peralta, F. Ogliaro, M. Bearpark, J. J. Heyd, E. Brothers, K. N. Kudin, V. N. Staroverov, R. Kobayashi, J. Normand, K. Raghavachari, A. Rendell, J. C. Burant, S. S. Iyengar, J. Tomasi, M. Cossi, N. Rega, J. M. Millam, M. Klene, J. E. Knox, J. B. Cross, V. Bakken, C. Adamo, J. Jaramillo, R. Gomperts, R. E. Stratmann, O. Yazyev, A. J. Austin, R. Cammi, C. Pomelli, J. W. Ochterski, R. L. Martin, K. Morokuma, V. G. Zakrzewski, G. A. Voth, P. Salvador, J. J. Dannenberg, S. Dapprich, A. D. Daniels, Ö. Farkas, J. B. Foresman, J. V. Ortiz, J. Cioslowski, D. J. Fox, Gaussian, Inc., Wallingford, CT, USA, **2009**.

[21] a) A. D. Becke, *J. Chem. Phys.* **1993**, *98*, 5648 – 5652; b) C. Lee, W. Yang, R. G. Parr, *Phys. Rev. B* **1988**, *37*, 785 – 789.

Received: September 26, 2014
Published online on ■■ ▮▮, 0000

K. A. Narayana, M. D. Casselman, C. F. Elliott, S. Ergun, S. R. Parkin, C. Risko, S. A. Odom**

■■ – ■■

***N*-Substituted Phenothiazine Derivatives: How the Stability of the Neutral and Radical Cation Forms Affects Overcharge Performance in Lithium-Ion Batteries**

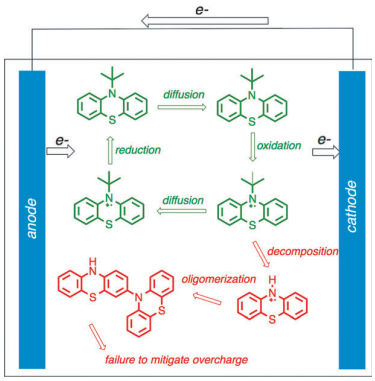

Redox shuttles are electrolyte additives that can prevent overcharge in batteries. They travel between the anode and cathode in their neutral and oxidized forms, mitigating excess current and stabilizing cell voltage. However, if the neutral or radical cation form of the shuttle decomposes, products can form that no longer protect the battery from overcharge, as is observed in the case of *N-tert*-butylphenothiazine.